Applied Catalysis B: Environmental 196 (2016) 77–88

Contents lists available at ScienceDirect

Applied Catalysis B: Environmental

journal homepage: www.elsevier.com/locate/apcatb

Photocatalytic activity of nitrogen doped TiO_2 nanotubes prepared by anodic oxidation: The effect of applied voltage, anodization time and amount of nitrogen dopant

Paweł Mazierski[a], Michał Nischk[a,d], Marta Gołkowska[a], Wojciech Lisowski[b], Maria Gazda[c], Michał Jerzy Winiarski[c], Tomasz Klimczuk[c], Adriana Zaleska-Medynska[a,d,*]

[a] Department of Environmental Technology, Faculty of Chemistry, University of Gdansk, 80-308 Gdansk, Poland
[b] Institute of Physical Chemistry, Polish Academy of Sciences, 01-224 Warsaw, Poland
[c] Department of Solid State Physics, Faculty of Applied Physics and Mathematics, Gdansk University of Technology, 80-233 Gdansk, Poland
[d] Department of Chemical Technology, Faculty of Chemistry, Gdansk University of Technology, 80-233 Gdansk, Poland

ARTICLE INFO

Article history:
Received 29 February 2016
Received in revised form 1 May 2016
Accepted 3 May 2016
Available online 6 May 2016

Keywords:
TiO_2 nanotubes
Nitrogen doping
Heterogeneous photocatalysis
Electrochemical oxidation

ABSTRACT

Nitrogen doped TiO_2 nanotube arrays were prepared by anodizing Ti foils in an organic electrolyte containing specified amounts of urea as nitrogen precursor. The photocatalytic activity of the samples was evaluated by analyzing the degradation kinetics of phenol in water. The influence of tubes' length, tubes' surface morphology and amount of nitrogen in the TiO_2 lattice on hydroxyl radical formation efficiency, photocatalytic activity and stability in four cycles was investigated. It was found that the photocatalytic activity as well as the charge carrier recombination rate depends on nitrogen concentration and the process parameters. 3.5 μm-long nanotubes containing 0.34 at.% of nitrogen seems to be favorable in phenol degradation and OH radicals generation under visible light. Comparison of XPS and photocatalytic activity test results shows decrease in phenol degradation efficiency with increasing amount of carbon contaminants on photocatalysts' surface.

1. Introduction

TiO_2 nanostructures, especially highly ordered nanotube arrays prepared by the anodization of titanium, have been widely used for recent years as photocatalysts due to their special features including unique structure, high specific surface area, better adsorption ability (comparing to powder photocatalysts) and unidirectional charge transfer [1–3]. TiO_2 nanotubes could be potentially used for photocatalytic degradation of pollutants in water [3,4] and gas [5] phases, inactivation of microorganisms [6], hydrogen production [7–9] and photoconversion of CO_2 [10]. However, major disadvantages of using TiO_2 nanotubes, which have not been fully overcome, are their relatively large band gap (3-3,2 eV) and high recombination rate of photogenerated electron–hole pairs [1,11]. These two major factors lead to low quantum yield of photocatalytic process and necessity to use of UV irradiation, which disables to apply them on an industrial scale. Many different strategies were proposed to solve these problems, such as transition metal cations doping [12,13], nonmetals doping [14–16], dye sensitization [17] and surface modification with noble metals and with low band gap semiconductors [18–20].

The incorporation of nonmetal atoms into the TiO_2 structure is still one of the most popular and effective method to enhance its photocatalytic performance. Among various investigated nonmetals, nitrogen attracts great attention since nitrogen atoms can be introduced into the TiO_2 lattice inducing a new N2*p* energy level above the valence band, thereby narrowing the band gap of TiO_2 and finally leading to a shift in the optical response towards visible range [21]. Furthermore, under UV irradiation, nitrogen atoms act as an efficient electron trap preventing electron–hole recombination [22]. It should be also noted that additional benefits from nitrogen doping of TiO_2 result from the fact that nitrogen have

* Corresponding author at: Department of Environmental Technology, Faculty of Chemistry, University of Gdansk, 80-308 Gdansk, Poland.
E-mail address: adriana.zaleska@ug.edu.pl (A. Zaleska-Medynska).

http://dx.doi.org/10.1016/j.apcatb.2016.05.006
0926-3373/

small ionization energy and atomic size comparable with oxygen, is stable and able to form metastable centers [23].

Nitrogen doped TiO_2 nanotubes could be prepared *via* various routes including ion implantation method [24,25], chemical bath deposition [26–30], ammonia annealing at low [31] and high temperatures [32,33], anodization of titanium in the electrolyte containing nitrogen precursor [34,35], and others [15,36–38]. Generally, all of these approaches can be classified into two categories: one and two-step synthesis processes. In the typical two-step route, amorphous TiO_2 nanotubes are obtained in the first step followed by nitrogen incorporation into the TiO_2 nanotubes in the second step, using immersing in hot ammonia solutions [29], annealing TiO_2 nanotubes with ammonia at high temperatures [26], by hydrothermal treatment of TiO_2 nanotubes [15] and by chemical vapor deposition [39]. Some of these methods, such as ion implantation, can cause strong structural alterations [40]. However, in view of industrial applications, two-step approach is cost intensive and operationally difficult [34]. In the one-step approach, nitrogen doped TiO_2 nanotube formation is mostly carried out using ethylene glycol-based electrolytes containing a small amount of nitrogen precursor, such as urea [34] and NH_4NO_3/NH_4OH [38] or by anodization of TiN alloy [36]. Recently, this method has been more and more popular as a straightforward, cost effective preparation process to produce nitrogen modified TiO_2 nanotubes of high purity at relatively low temperature. Antony et al. [34] prepared nitrogen doped TiO_2 nanotubes by anodization of Ti foil in the electrolyte composed of NH_4F, water, ethylene glycol and urea. The effect of nitrogen concentration on the optical band gap was investigated. They showed that nitrogen atoms are incorporated into TiO_2 structure in two forms: substitutional and interstitial. They also showed that band gap value of nitrogen doped TiO_2 nanotubes depends on the amount of nitrogen precursor. Kim et al. [36] obtained nitrogen doped TiO_2 nanotubes by anodization of TiN alloy in the glycerol-based electrolyte. Photocurrent experiment showed that nitrogen doped sample have lower and higher photoresponse under the influence of UV and visible light irradiation compared to undoped one, respectively. Shankar et al. [38] prepared nitrogen doped TiO_2 nanotubes by one-step approach in the electrolyte containing HF, NH_4NO_3 and ammonium hydroxide. Nitrogen doped samples exhibited enhanced optical absorption in the wavelength range of 400–510 nm.

Generally it could be concluded that photocatalytic activity of powder TiO_2 under the UV and visible light irradiation is strongly dependent on the amount of nitrogen incorporated into the bulk phase of TiO_2 [21], while the photoactivity of undoped TiO_2 nanotubes under UV irradiation mainly depends on the tubes' parameters (length and wall thickness) [1,5]. On the other hand, in most reports photocatalytic activity of nitrogen modified TiO_2 nanotubes were measured using dyes as model substances on photodegradation tests [28,30,37]. Dyes are not recommended to be used as model compounds due to their absorption properties (dye sensitization), large photoabsorption coefficient and complicated mechanism of degradation [41].

In view of this, we have recently obtained nitrogen doped TiO_2 nanotubes prepared *via* one-step electrochemical method under various conditions of anodization process (U = 20-50 V and t = 30–120 min). For the first time, the morphology of nitrogen doped TiO_2 nanotubes, as well as the chemical character and nitrogen content were related to the efficiency of electron-hole recombination process, efficiency of phenol degradation and hydroxyl radicals formation under both UV and Vis irradiation. Additionally, the influence of carbon-like surface contaminants on the photocatalytic activity of nitrogen doped TiO_2 nanotubes was studied. A possible mechanism of pollutants degradation on the surface of nitrogen doped TiO_2 nanotubes under visible light was proposed as well.

2. Experimental

2.1. Preparation of nitrogen doped TiO_2 nanotubes

Prior to anodization, the Ti foils were ultrasonically cleaned in acetone, isopropanol, methanol and deionized water (each solvent 10 min) and dried in air stream. The anodization was carried out using a two-electrode system with Ti foil as anode and platinum mesh as cathode. The distance between the electrodes was kept constant at 2 cm. Ag/AgCl reference electrode was used only for controlling the process and obtaining information about actual potential of Ti working electrode. All anodizations were carried out at room temperature. The anodization took place in the electrolyte composed of ethylene glycol (EG) with 2 vol% water, containing 0.09 M NH_4F and different weight percentage of urea, used as nitrogen precursor. Ti foil was anodized for 30–120 min at the applied voltage from the range of 20–50 V using programmable DC power supply (MANSON SDP 2603). Finally, the obtained samples were rinsed with deionized water, sonicated in water (5 min), dried in air (80 °C for 24 h) and calcined at 450 °C (heating rate 2 °C/min) for 1 h.

2.2. Characterization of nitrogen doped TiO_2 nanotubes

The morphology of obtained undoped and nitrogen doped TiO_2 nanotubes was determined by using scanning electron microscopy (SEM, FEI Quanta 250 FEG). Crystal structure of prepared samples was determined from X-Ray diffraction patterns (XRD) measured in the range of 2θ = 20–80, using X-ray diffractometer (Xpert PRO-MPD, Philips) with copper Kα radiation (λ = 1.5404 Å). The XRD estimation of the crystallite size was based on the Scherrer formula. All XPS spectra were recorded on PHI 5000 VersaProbe™ (ULVAC-PHI) spectrometer with monochromatic Al Kα radiation ($h\nu$ = 1486.6 eV). X-ray beam was focused to diameter 100 μm, measured area was defined as a 250 μm square. Both the survey and high-resolution (HR) XPS spectra were collected with the hemispherical analyzer at the pass energy of 117.4 and 23.5 eV and the energy step size of 0.4 and 0.1 eV, respectively. The UV–vis reflectance and absorbance spectra of undoped and nitrogen doped TiO_2 nanotubes were recorded on Shimadzu UV–Vis Spectrophotometer (UV 2600) equipped with an integrating sphere. The baseline was determined using barium sulphate as a reference. The spectra were registered in a range of 300–800 nm, with a scanning speed of 250 nm/min at the room temperature. Bandgap energy values were obtained as the intercept of the tangent of the Kubelka-Munk function transformation plot ($F_{KM}{}^{0,5}E_f{}^{0,5}$) vs. photon energy. The photoluminescence (PL) measurements were carried out at room temperature using LS-50B Luminescence Spectrophotometer equipped with Xenon discharge lamp as an excitation source and a R928 photomultiplier as detector. The excitation radiation (360 nm) was directed on the sample's surface at an angle of 90°.

2.3. Measurement of photocatalytic activity

Photocatalytic activity of undoped and nitrogen doped TiO_2 nanotubes was determined in two model processes: cleaning of water from phenol and •OH radicals generation efficiency (using terephthalic acid). Phenol was selected as a model pollutant because it is a nonvolatile and common contaminant present in industrial wastewaters [42]. Terephthalic acid reacts with hydroxyl radicals to form highly fluorescent product: 2-hydroxyterephthalic acid. The photocatalytic activity tests were carried out in a photoreactor made of quartz with the working volume of about 15 mL. The phenol and terephthalic acid concentration was 0.21 mM and 0.5 mM, respectively. The samples with the surface area of 4 cm^2 were immersed in phenol or terephthalic acid solution for 30 min

in the dark in order to achieve adsorption-desorption equilibrium. Subsequently, the reaction system was irradiated with a 1000 W Xenon lamp (Oriel 66021) under magnetic stirring (500 rpm). For the visible-light activity tests, the light beam was passed through GG420 filter to cut-off wavelengths shorter than 420 nm. A reference phenol and terephthalic acid sample (0.5 mL) were taken just before starting irradiation and subsequent samples (0.5 mL) were collected at regular time periods (20 min) during irradiation. Phenol concentration was estimated by the colorimetric method after derivatization with *p*-nitroaniline using UV–vis spectrophotometer (λ = 480 nm). Fluorescence spectra were recorded at room temperature by using a LS-50B Luminescence Spectrophotometer equipped with Xenon discharge lamp as an excitation source (excitation wavelength 315 nm) and a R928 photomultiplier detector.

3. Result and discussion

3.1. Formation and morphology of nitrogen doped TiO_2 nanotubes

Top view images of selected samples are shown in Fig. 1. The nanotubes' dimensions estimated based on SEM images are given in Table 1. All synthesized nanotubes are smooth and vertically oriented but their surface is covered with small amount of impurities (Fig. 2) consisting of hydrous titanium oxides created as a consequence of hydrolysis of TiO_2 during anodization [5]. Furthermore, nanotubes obtained with higher voltages and longer anodization time (2 h) are more uniform (no significant differences in nanotubes' length was observed over the entire observed area) and longer as compared to nanotubes obtained with lower voltages and shorter anodization time. As shown in Fig. 2, oxide ripples on the outer wall of nanotubes are not observed due to low water content in the electrolyte (less than 2 wt%) [43]. The dimensions of nanotubes can be easily controlled in a wide range by changing the applied voltage and anodization time. The internal and external diameter and length of nanotubes increased with increasing applied potential and anodization time, starting from about d = 54 nm and l = 0.8 μm (20 V) and reaching about d = 96 nm and l = 3.8 μm (see details in Table 1). It should be also noted that dimensions of all nitrogen doped TiO_2 nanotubes are larger in comparison to undoped ones prepared under the same conditions (see details in Table 1). Diameter and length of nitrogen doped TiO_2 nanotubes rose from d = 61 nm and l = 1.0 μm up to d = 114 nm and l = 6.8 μm. Thus, application of the same anodization conditions (U = 50 V, t = 1 h) in the presence of urea (0.2 wt%) resulted in 2 times larger diameter and 2.5 times increase in length. The developed surface areas calculated based on [44] of all obtained samples are summarized in Table 1.

Fig. 2 shows current density-time curve recorded during anodization of selected undoped and nitrogen doped TiO_2 nanotubes. Current density-time behavior can be ascribed to different stages in the nanotubes formation process [45]. Comparing current density-time curves' registered for undoped and nitrogen doped sample, a significant difference in their shapes was observed. As it can be seen in Fig. 2, current density-time curve of nitrogen doped TiO_2 nanotubes is located below the curve of undoped sample which suggests limited ionic mass transport of the formed oxide layer. Furthermore, nitrogen doped sample present broader stage II, compared to undoped one, indicating that pore formation is prolonged and formation and dissolution of nitrogen doped TiO_2 nanotubes slows down. Thus, increase of wall thickness of the nitrogen doped nanotubes can be described with the slower chemical dissolution rate of the oxide layer. And finally, the current density recorded during anodization of nitrogen doped sample reached a quasi-steady state (last stage III) faster than for undoped sample.

Table 1
Sample labels, characterization and photocatalytic activity of pristine and nitrogen doped TiO_2 nanotubes.

Sample label	Urea concentration (wt.%)	External diameter (nm)	Nanotubes length (μm)	Wall thickness (nm)	Developed surface area[a] (cm^2)	Band gap (eV)	Average crystallite size (nm)	Photocatalytic degradation of phenol			
								Initial reaction rate, r (μmol dm^{-3} min^{-1})		Reaction rate constant, k (min^{-1})	
								UV–vis	Vis	UV–vis	Vis
NT_20V_1h	0	54	0.8	6	285	3.30	33	1.86	0.05	0.0065	0.0004
NT_30V_1h		65	1.7	6	549	3.20	35	2.02	0.16	0.0077	0.0005
NT_40V_1h		72	2.2	6	646	3.06	36	4.25	0.37	0.0216	0.0009
NT_50V_1h		78	2.7	14	689	2.95	36	2.13	0.27	0.0096	0.0007
NT_40V_0.5h		66	1.6	6	492	3.08	33	2.10	0.11	0.0077	0.0005
NT_40V_2h		96	3.8	11.5	745	3.03	38	2.23	0.12	0.0084	0.0006
N—NT_0.2%_20V_1h	0.2	61	1.0	10.5	266	3.20	30	2.13	0.27	0.0078	0.0009
N—NT_0.2%_30V_1h		76	2.0	11	464	3.08	29	2.34	0.69	0.0099	0.0022
N—NT_0.2%_40V_1h		89	3.5	10.5	757	2.94	27	4.53	1.33	0.0247	0.0046
N—NT_0.2%_50V_1h		114	6.8	9.5	1285	2.80	37	3.45	1.01	0.0180	0.0033
N—NT_0.2%_40V_0.5h		70	1.6	7	461	2.90	32	2.39	0.53	0.0084	0.0017
N—NT_0.2%_40V_2h		112	4.8	13.5	814	2.84	31	3.72	1.06	0.0201	0.0032
N—NT_0.1%_40V_1h	0.1	72	3.5	4.5	1111	3.00	33	4.25	0.96	0.0214	0.0028
N—NT_0.3%_40V_1h	0.3	63	3.4	4.5	1111	2.90	33	4.36	0.80	0.0223	0.0031
N—NT_0.5%_40V_1h	0.5	71	3.4	6	1017	2.75	34	4.09	0.48	0.0200	0.0019

[a] estimated total surface area of whole TiO_2 nanotube arrays on the flat surface (4 cm^2)(calculated based on Ref. [42]).

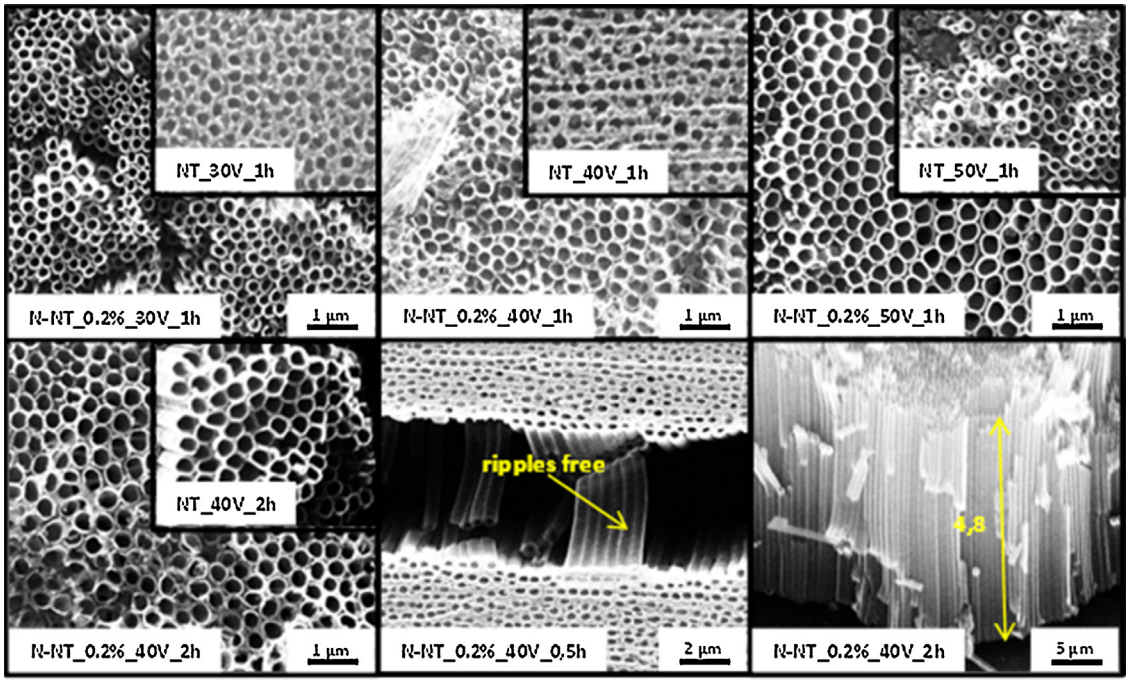

Fig. 1. Top view and cross section images of selected nitrogen doped TiO_2 nanotubes.

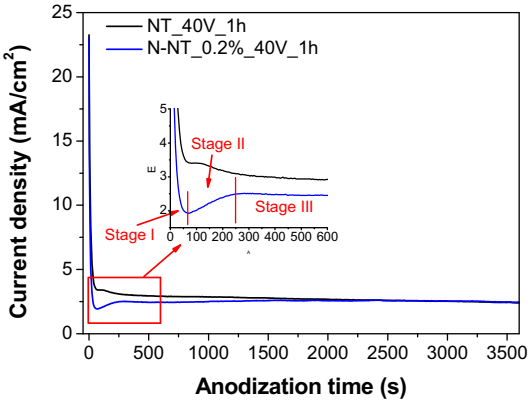

Fig. 2. Current density-time curve for nitrogen doped TiO_2 nanotubes formation process.

It is known that the final stage of anodic oxidation determines the nanotube length [46]. In the case of nitrogen doped sample, stage III was prolonged which resulted in the longer length of nitrogen doped nanotubes compared to undoped ones. Such phenomenon was observed for other nitrogen doped TiO_2 nanotubes obtained by using different anodization conditions (not included in Fig. 2). This phenomenon may be associated with the addition of urea to the electrolyte which causes an increase of the pH of the solution ($\Delta pH \approx 0.7$). It is known that with increasing of pH the hydrolysis rate increases, which slows down the rate of chemical dissolution. Furthermore, it was reported that longer nanotubes can be formed in solution with higher pH compared with acidic solutions [47] (which is consistent with our observations).

3.2. Chemical composition of nitrogen doped TiO_2 nanotubes

The elemental composition and chemical character of undoped and nitrogen doped nanotubes was analyzed by XPS. The results are shown in Figs. 3 and 4 and Table S1–2 (Supporting materials).

Two similar chemical states of titanium were separated after deconvolution of Ti 2p spectra of both undoped and nitrogen doped TiO_2 nanotubes. The representative Ti $2p_{3/2}$ peaks at binding energy (BE) of 459.5 eV and 458 eV are characteristic for anatase phase of TiO_2 materials [48,49] and can be identified as Ti^{4+} and Ti^{3+}, respectively [42]. Three chemical states of oxygen were separated in O 1s spectra recorded for all samples. The first one at BE of 530.7 eV is characteristic for oxygen in the TiO_2 crystal phase, the second state at BE of 531.8 eV can be assigned to surface TiOx species, OH groups binding with two Ti surface atoms and C=O [42,50]. For nitrogen doped TiO_2 nanotubes the presence of Ti—O—N species was also considered [51]. The last state, at BE of 532.8 eV, can be originated from surface oxygen in Ti—OH and C—OH [42,50]. Five carbon peaks identified in C 1s spectra can be assigned to sp2, sp3, C—OH, C=O, O=C—O species and C—N (for nitrogen doped samples) [52,53]. The nitrogen surface species were evidently detected in the N 1s XPS spectra. As shown in Figs. 3–4 a strong signal at 400.7 eV appears in the N 1s region for the relatively small content of nitrogen (about 0.2 at.%). Similar single XPS state of nitrogen was reported by other authors for nitrogen doped TiO_2 nanotubes [51,54] and other nitrogen doped TiO_2 nanocatalysts [55–58]. Taking the BE value, the simple formation of TiN and NOx surface species can be excluded [53]. Following the experimental XPS data reported in literature it is likely that Ti—O—N and/or Ti—N—O bonds are formed by nitrogen introducing into TiO_2 lattices by substitution at the sites of the oxygen atoms [51,54–57].

In undoped TiO_2 nanotubes, the relative contribution of Ti^{4+} states is dominant, since the content of Ti^{3+} component differs from 2 to 3% of total Ti in surface layer. The sample anodized at 20 V reveals a large contribution of sp2 carbon species what indicates the formation of graphite-like carbon contaminants on the top of TiO_2 nanotubes (see Table S1). In the case of nitrogen doped samples, the Ti^{4+} state of titanium is also dominant and accompanied by 2–3.3% contribution of Ti^{3+} fraction. No XPS signals evidenced the formation of Ti—N species were detected. However the analysis of the HR N1s XPS spectra indicated that nitrogen was doped effectively (Figs. 3–4, Table S2,), probably in the chemical environment of Ti—O—N and/or O—Ti—N species

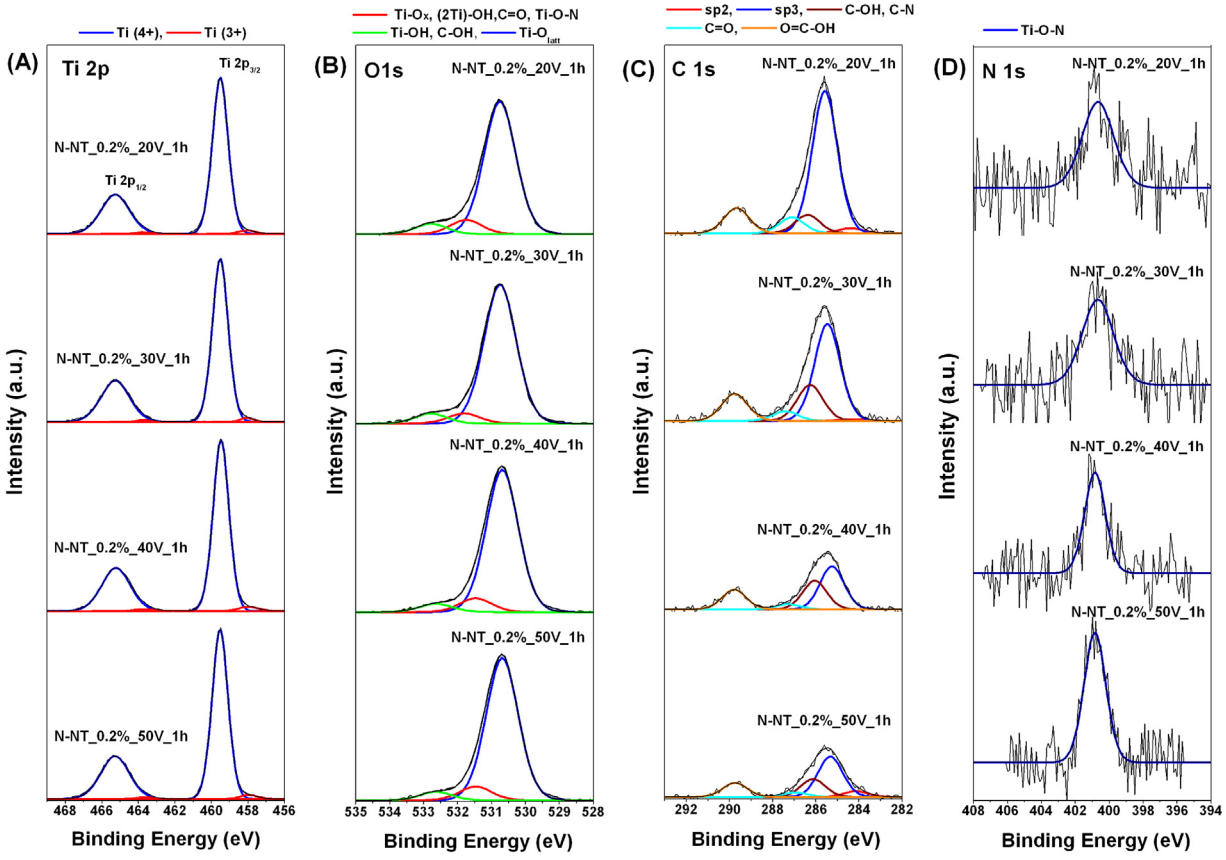

Fig. 3. The HR XPS spectra of Ti2p, O1s, C1s and N1s of nitrogen doped TiO_2 samples obtained using different voltages (20 V–50 V).

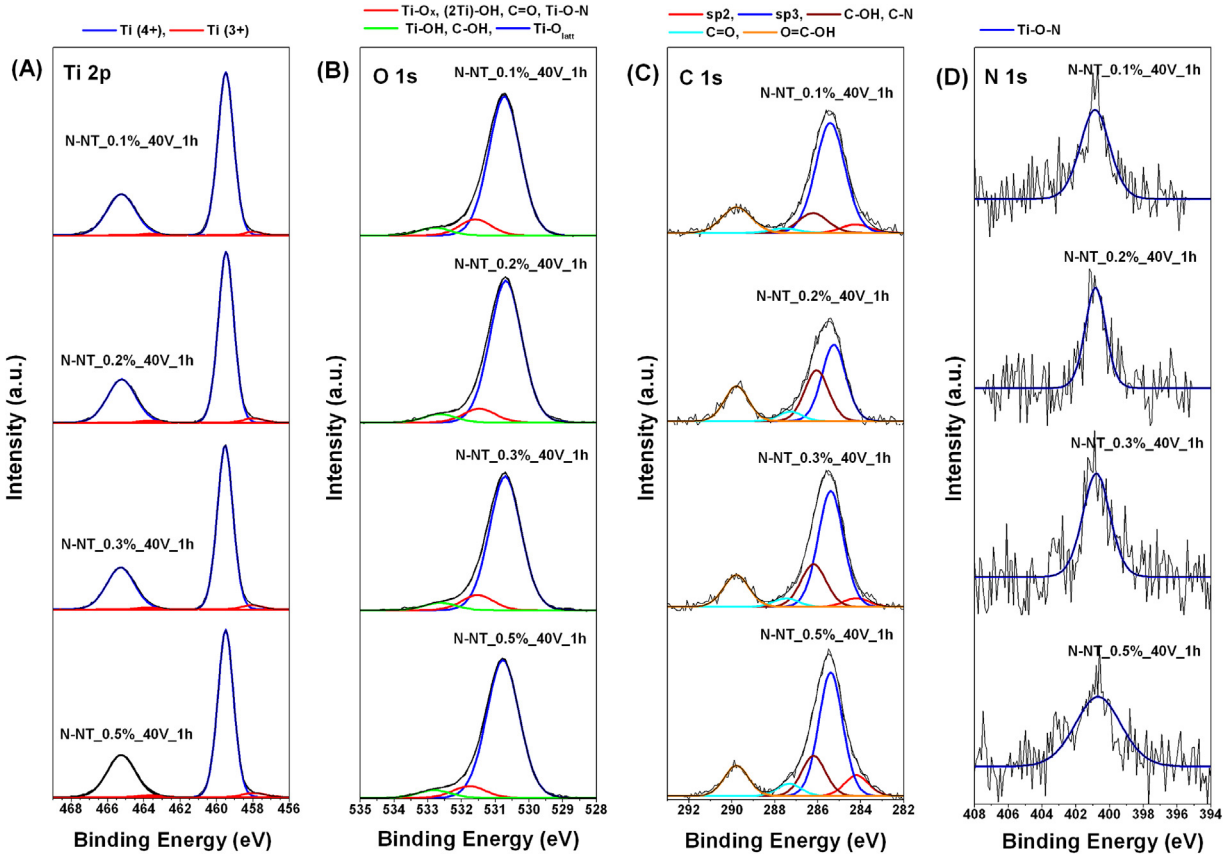

Fig. 4. The HR XPS spectra of Ti2p, O1s, C1s and N1s of nitrogen doped TiO_2 samples obtained with different nitrogen content (0.1%–0.5%).

[51,54–57]. The surface content of nitrogen species agree well with the amount of nitrogen precursor used for doping (Table S2). The carbon content in the nitrogen doped samples was found to be lower compared to undoped nanotubes anodized at the same conditions and decreased as anodization voltage increased. This phenomenon could be explained as a result of rearrangement of the form of carbon-originated substances on the surface of nanotubes, which is induced by nitrogen doping. The results show that the relation between the fraction sp2/sp3 and the fraction corresponding to BE of 532.8 eV (among others C—N species) has been changed for nitrogen doped samples. Same of carbon-originated species, which are weakly bound to the surface of nanotubes, may be removed by nitrogen doping. However it should be emphasized that all samples were analyzed by XPS 4–5 weeks after preparation. Thus it is supposed that carbon states, which can be formed as a results of preparation procedure, can be affected by carbon-like surface contaminants, originated from air. To elucidate this point all nitrogen doped TiO_2 samples were analyzed again after the next 10 weeks from the first XPS analysis. The results, (presented in Table S2) revealed significant increase of carbon content (7.1 ± 1.8 at.%). That indicates high activity of TiO_2 nanotubes against of air carbon-like contaminants and makes quantitative interpretation of fractional distribution of carbon states rather doubtful. Nevertheless, it should be also noted that the most photoactive sample, N—NT_0.2%_40V_1 h, exhibited relatively low total contents of carbon (6.8 at.%), which was distributed mainly in form of sp3 (44.5%), C—OH (29.7%), carboxyl (20.4%) and C=O species (5.5%).

3.3. Optical and photoluminescent properties of nitrogen doped TiO_2 nanotubes

Absorbance curves and the Kubelka-Munk function transformation plot vs. photon energy of all samples are presented in Fig. S1 (Supporting materials). The typical absorption in the UV region (attributed to trapped holes at the lattice oxide ion sites, O—) and the broad band in the range of 400–800 nm (associated with trapped electrons at the Ti^{3+} center) was observed for all samples [30,59]. Furthermore, for almost all nitrogen doped TiO_2 nanotubes, the absorbance in the UV region was lower compared to undoped ones obtained in the same anodization conditions except for samples containing 0.22 (N—NT_0.1%_40V_1 h) and 0.34 at.% (N—NT_0.2%_40V_1 h) of nitrogen which exhibited higher absorbance in the UV region than sample NT_40V_1 h. These phenomena were observed for nitrogen doped TiO_2 nanotubes obtained by using different doping strategies [15,27]. As it can be seen in Table 1 (and Fig. S1), the bandgap energy for undoped TiO_2 nanotubes decreased with increasing the applied voltage and anodization time. It is expected that undoped TiO_2 nanotubes calcined in 450 °C are composed mainly of anatase phase (band gap energy 3.23 eV). However, for undoped nanotubes obtained under 20 V, the estimated bandgap energy was higher, reaching 3.3 eV. This is not surprising and can be attributed to the quantum-size effect of TiO_2 nanotubes and was already observed by Mor et al. [60]. For all undoped samples obtained under higher voltages, the bandgap was lower (2.95–3.20) than in the case of pure anatase. The narrowing of bandgap energy of undoped TiO_2 nanotubes can be attributed to the presence of structural defects, sub-band states, Ti^{3+} states and oxygen vacancies in the nanotubes. Ti^{3+} states may cause the appearance of impurity states located below (about 0.1–0.8 eV) conduction band, which enhances the visible light response [22]. Correlation between band gap value and Ti^{3+} content was confirmed by XPS analysis (see Table S1 from Supporting materials). Sample exhibiting lower band gap ($E_g = 2.95$ eV) contains higher amount of Ti^{3+} species in the surface layer (3.02 at.%).

All nitrogen doped samples showed a red shift (compared to undoped samples obtained under the same conditions) suggesting that their bandgap energy is narrowed. The narrowing of bandgap energy could be attributed to the interaction between the N2*p* and O2*p* orbital electron states and to the excitation of electrons from localized N2*p* level within the bandgap [35] and consequently under visible light [15]. Nevertheless, our result show that bandgap energy also depends on the nitrogen content in the TiO_2 lattice and decreased with increasing of nitrogen content (what is in agreement with literature [22]).

Photoluminescence spectra of all samples are presented in Fig. 5. The emission peak at 421 nm can be ascribed to the existence of self-trapped excitons from TiO_6^{8-} octahedron [61]. The emission peaks at 449 and 484 nm could be assigned to the presence of surface defects, such as oxygen vacancies, which creates intermediate energy states located below the conduction band, and, which are able to trap electrons while the peak at 530 nm can be associated with radiative recombination of charge carriers [62]. PL intensity registered for undoped samples decreased with increasing anodization potential and time. Two explanations are probable for this phenomenon. First, undoped nanotubes, obtained with higher voltages and longer anodization time, are more uniform and their surface is smoother as compared to nanotubes obtained with lower voltages and shorter anodization time. Well-aligned (with the same length and without partially damaged) and well-separated (for example, without oxide rings) TiO_2 nanotubes can provide a direct and rapid pathway for charge transport, decreasing the carrier path length and as a consequence reduces recombination losses (reduced number of recombination centers). Second, the lower PL intensity for undoped samples, anodized with increased potential and time, may be associated with generation of higher amount of structural defects, sub-band states, Ti^{3+} states and oxygen vacancies, facilitating electron–hole separation and promoting the interfacial electron transfer process. It is likely that during the calcination step a higher amount of oxygen vacancies is induced in the TiO_2 nanotubes as a result of carbon removing [63]. It is known that carbon is incorporated into TiO_2 nanotubes during the anodization in the organic electrolytes. Higher anodization voltage can cause the higher content of carbon and consequently more oxygen vacancies after the calcination step (for given temperatures). Furthermore, PL intensity for nitrogen doped TiO_2 nanotubes obtained under different voltages and anodization time (samples exhibited constant amount of nitrogen dopant, ≈0.33 at.%), was lower compared to undoped nanotubes obtained under the same conditions. These results suggest that nitrogen doping promotes the efficiency of charge carrier separation rate and was already observed [14,64,65]. As shown in Fig. 5c, electron–hole recombination rate depended on the nitrogen content in the TiO_2 lattice. Nitrogen doped TiO_2 nanotubes obtained with different nitrogen content (in the range of 0.22–0.5 at.%) exhibited lower PL intensities compared to undoped ones. The lowest emission intensity was observed in the case of TiO_2 nanotubes containing 0.34 at.% of nitrogen (N—NT_0.2%_40V_1 h).

3.4. Structural properties of nitrogen doped TiO_2 nanotubes

The XRD patterns for the all obtained samples are demonstrated in Supplementary materials Fig. S2. In all patterns, reflections of anatase and titanium support can be seen. The intensity of the anatase reflections increased while these of the substrate decreased with the increase of anodization voltage and time. It is caused by increasing length of the nanotubes which leads to an increase of the thickness of the nanotube layer. In the patterns of the samples anodized at 20 V, a very weak reflection of rutile is present (undistinguishable in the scale of Fig. S2). The patterns of the undoped and nitrogen doped TiO_2 nanotubes prepared with the same anodiza-

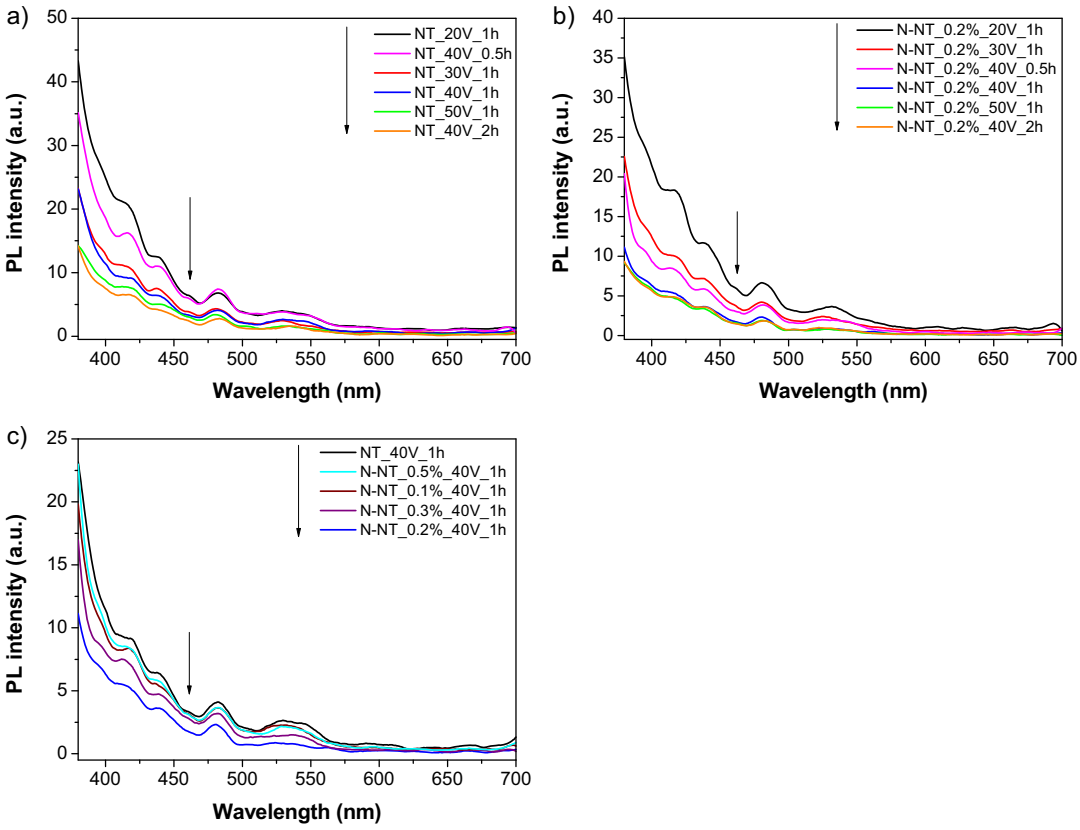

Fig. 5. Photoluminescence spectra of pristine and nitrogen doped TiO_2 nanotubes.

tion voltage and time are similar one to another. Moreover, the concentration of nitrogen in the TiO_2 lattice did not significantly influence the XRD patterns (Fig. S2c). The average crystallite size of the nanotubes (see Table 1) were estimated on the basis of the (101) reflection width. In the case of undoped samples, the crystallite size increased with increasing of anodization voltage (in the range of 20–40 V) and time (30–120 min), what is in agreement with literature [66]. The crystallites of undoped nanotubes are significantly larger than these of nitrogen doped and it was already observed [26]. For nitrogen doped nanotubes, neither anodization time nor urea concentration influences significantly the crystallite sizes. Crystallite size decreased with increasing of anodization voltage in the range of 20–40 V. In the case of samples exhibited different content of nitrogen in the TiO_2 lattice, crystallite size increased gently with increasing amount of nitrogen (in the range of 0.34–0.5 at.%) from 27 to 34 nm. Crystallite size calculated by Scherrer equation provides us also information about the stresses in the crystal lattice. Greater amount of nitrogen in the unit cell may result in increased stresses and as a consequence lead to changes in "crystallite sizes".

3.5. Correlation between properties and photocatalytic activity of undoped and nitrogen doped TiO_2 nanotubes

The photocatalytic activity (presented as initial reaction rate and rate constant, Table 1) and stability of all obtained samples were studied in the process of photocatalytic decomposition of phenol and •OH radicals generation efficiency under the influence of UV–Vis and visible light irradiation. During preliminary experiments, phenol solutions were irradiated with the absence of photocatalyst in order to define the influence of photolysis on the phenol decomposition process. After 60 min of irradiation the decomposition of phenol under UV–Vis and Vis was equaled 3 and 1% respectively. For •OH radicals generation tests, PL peaks were not observed (both under UV–Vis and visible light irradiation) in the absence of photocatalyst, which suggests that the product possessing fluorescence properties is generated by chemical reaction on the photocatalyst/water interface via photocatalysis.

A good correlation between degradation efficiency of phenol and generation of •OH radicals was observed. The photoactivity of all samples depends on their preparation conditions (under both UV–Vis and Vis irradiation), namely increased with increasing anodization voltage and time in the range of 20–40 V and 30–60 min, as shown in Table 1 and Fig. 6. The highest phenol decomposition rate constant (reached 0.0216 and 0.0009 min^{-1} for undoped sample and 0.0247 and 0.0046 min^{-1} for nitrogen doped sample under UV–Vis and Vis irradiation, respectively) and generated •OH radicals was observed for samples anodized at 40 V by 60 min, while in the case of samples anodized longer than 60 min and at voltage higher than 40 V photocatalytic activity significantly decreased. Macak et al. [67] suggested that photocatalytic activity of undoped TiO_2 nanotubes under the influence of UV irradiation depends on tubes length, namely the longer TiO_2 tubes, the higher is their photocatalytic activity due to more efficient total light absorption and lower recombination of charge carriers. In our case, a clear correlation between tubes length and photocatalytic activity was not observed; undoped and nitrogen doped tubes with the largest length (NT_50V_1 h and N—NT_0.2%_50V_1 h) exhibited lower activity in phenol decomposition than shorter nanotubes (NT_40V_1 h and N—NT_0.2%_40V_1 h). Additionally, this relationship was observed not only for UV–Vis but also for visible light. Furthermore, all nitrogen doped samples showed enhanced photoactivity (increase at an average rate about of 50% under UV–Vis light) compared to undoped samples prepared under the same preparation conditions (despite the larger dimensions of nitrogen doped samples). As mentioned before, the charge carrier separa-

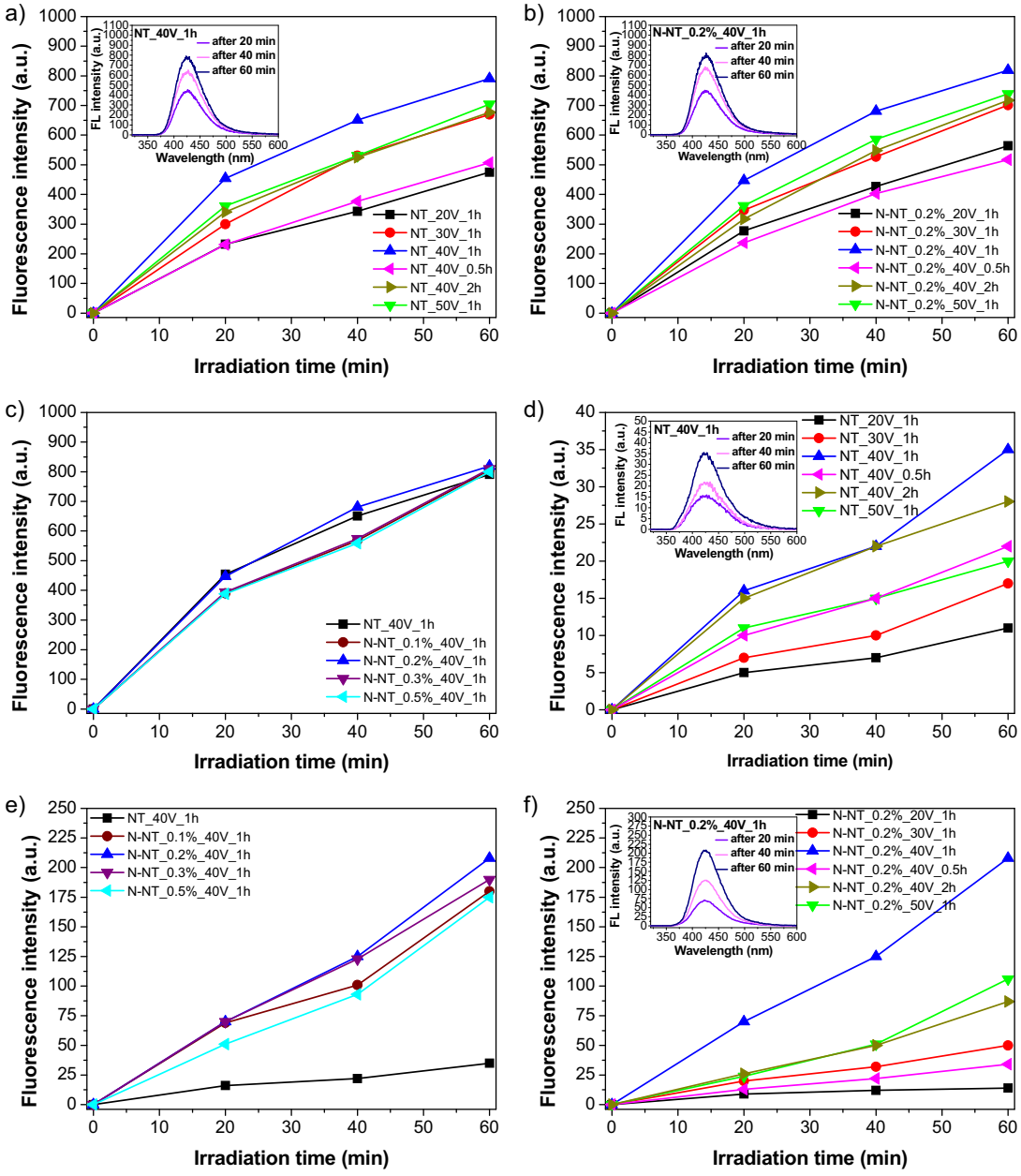

Fig. 6. Efficiency of hydroxyl radicals (•OH) generation of on the surface of pristine and nitrogen doped TiO_2 nanotubes illuminated with UV–Vis (a–c) and Vis (d–f) irradiation.

tion rate is improved for samples doped with nitrogen (see Fig. 5), and thus photocatalytic activity is also enhanced. The most photoactive sample (N—NT_0.2%_40V_1 h) exibited more than five times higher phenol decomposition rate constant under Vis irradiation compared to undoped sample (NT_40V_1 h).

For nitrogen doped TiO_2 nanotubes, the photocatalytic properties and charge carriers recombination rate were strictly correlated and depended not only on anodization parameters (time and voltage) but also on the amount of nitrogen (and resulting nitrogen concentration in TiO_2 bulk). Samples containing 0.34 at.% of nitrogen (N—NT_0.2%_40V_1 h) exhibited the highest photoactivity (reached r = 4.53 and 1.33 μmol dm^{-3} min^{-1} and k = 0.0247 and 0.0046 min^{-1} under UV–Vis and Vis irradiation, respectively). Furthermore, photocatalysts containing 0.22 (N—NT_0.1%_40V_1 h) and 0.5 at.% of nitrogen (N—NT_0.5%_40V_1 h) showed lower ability to degrade phenol and generate •OH radicals compared to samples containing 0.38 (N—NT_0.3%_40V_1 h) or 0.34 at.% of nitrogen. The lowest photoactivity was observed for samples containing 0.5 at.% of nitrogen (almost three times lower photoactivity under Vis irradiation compared to the most photoactive sample).

The most photoactive samples, both undoped (NT_40V_1 h) and nitrogen doped TiO_2 nanotubes (N—NT_0.2%_40V_1 h) were chosen for performing stability tests in four subsequent measurement cycles under UV–Vis and Vis irradiation, as shown in Fig. 7c–d. The photoactivity of both samples decreased in subsequent measurement cycles, which suggests that surface of TiO_2 may have been blocked by phenol partial decomposition products. Nitrogen doped sample showed better stability (photoactivity loss of about 1% in subsequent cycles under UV–Vis irradiation) compared to undoped one (photoactivity loss of about 3% in subsequent cycles under UV–Vis irradiation), which may be related to its better activity in first measurement cycle and consequently with better efficiency in phenol degradation byproducts removal. Hence, small part of the photocatalyst's surface are blocked in the initial stage of second and subsequent measurement cycles. In comparison, the surface of less active, undoped TiO_2 nanotubes remain partially clogged after

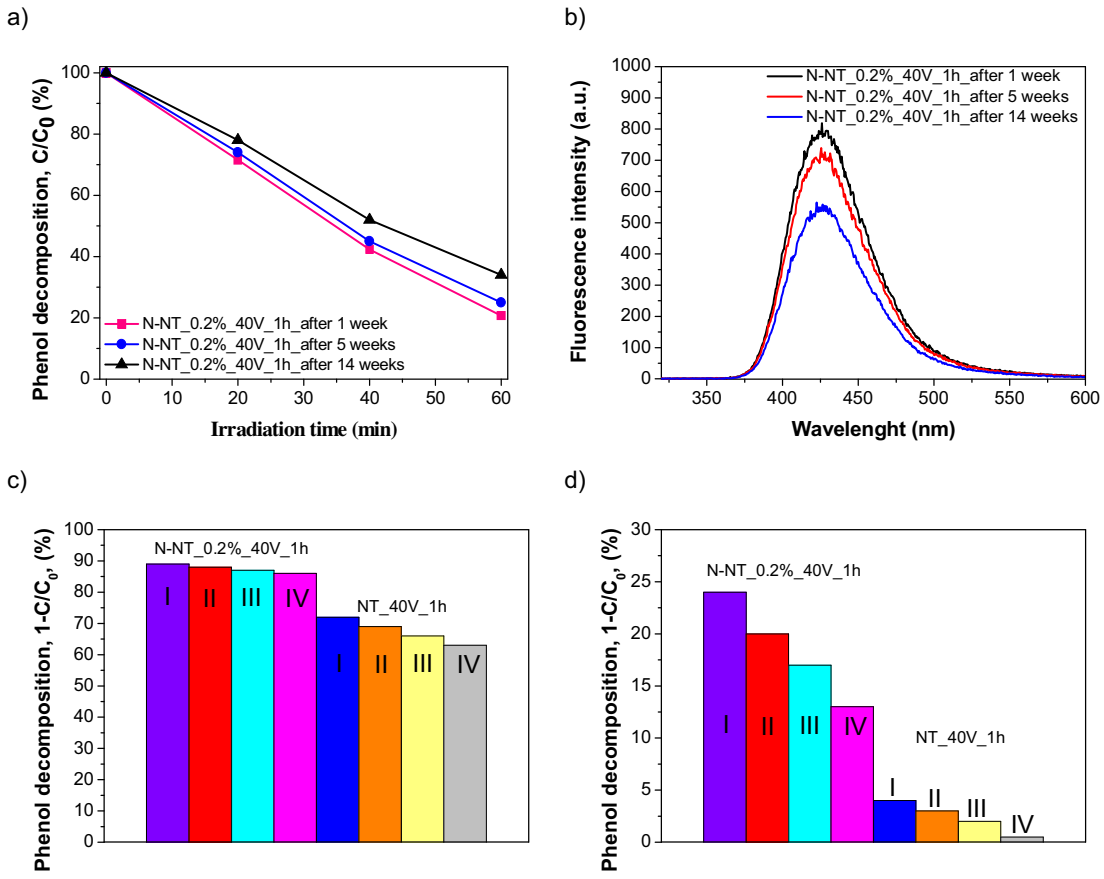

Fig. 7. The effect of storage time on stability of nitrogen doped TiO_2 nanotubes: (a) efficiency of phenol degradation over the N—NT_0.2%_40V_1 h sample after 1, 5 and 14 weeks from the moment of sample's preparation; (b) efficiency •OH radicals generation over the N—NT_0.2%_40V_1 h sample after 1, 5 and 14 weeks from the moment of sample's preparation; (c) efficiency of phenol degradation under UV–vis light in the presence of pristine and nitrogen doped TiO_2 nanotubes in four subsequent degradation cycles; and (d) efficiency of phenol degradation under Vis light in the presence of pristine and nitrogen doped TiO_2 nanotubes in four subsequent degradation cycles.

the first measurement cycle and this blocking process progresses in subsequent cycles leading to decrease of activity. In contrast, to confirm this theory, •OH radicals generation tests (the example of photocatalytic process in which easily adsorbable byproducts are not created) were performed. It was found that the amount of generated •OH radicals in subsequent cycles was invariable for both undoped and nitrogen doped nanotubes (results are not presented).

3.5.1. *The influence of carbon-like surface contaminants on the photocatalytic activity*

As previously mentioned, undoped and nitrogen doped samples have ability to absorb carbon contaminants from air (see Table S1–2 and description in Section 3.4). To determine the influence of adsorbed carbon compounds on photocatalytic activity, the most active sample (N—NT_0.2%_40V_1 h) was examined after specified time intervals (1, 5 and 14 weeks) from the moment of its preparation in the process of phenol decomposition under the influence of UV–Vis irradiation. These results are presented in Fig. 7a. The sample (N—NT_0.2%_40V_1h_after 14 weeks) showed slightly lower activity, as degradation efficiency after 60 min of irradiation reached about 66%. Comparing the XPS data and photocatalytic activity test results, it can be concluded that phenol decomposition efficiency decreased with increasing amount of carbon contaminants on photocatalyst's surface. This could be explained by the fact that adsorbed carbon contaminants can block the photocatalyst's surface, as a consequence, can cause decrease in its activity (in our case, increase of carbon compounds of about 80% caused a decrease of photoactivity of about 14%). To confirm this theory, •OH radicals generation tests in the presence of this samples were performed. It was found that the amount of generated •OH radicals (which are responsible for the degradation of phenol) decreased with increasing amount of carbon contaminants on photocatalyst's surface, as shown in Fig. 7b.

3.5.2. *Mechanism of visible light driven degradation of phenol*

In order to summarize previously discussed experimental data, the charts presenting the photocatalytic activity of nitrogen doped TiO_2 nanotubes under Vis irradiation as a function of nanotubes' length and nitrogen content were prepared. Fig. 8a presents the relation between photocatalytic activity and nanotubes' length in the case of constant amount of nitrogen dopant (≈0.33 at.%, confirmed by XPS analysis). The difference in nanotubes' length was achieved by varying anodization voltage in the range of 20–50 V. Photocatalytic activity increased with increasing the length of nanotubes, reaching maximal value (r = 1.33 μmol dm^{-3} min^{-1}) for the length of 3.5 μm. Further extension of nanotubes' length (l = 6.8 μm) caused the decrease in activity (r = 1.01 μmol dm^{-3} min^{-1}). Initial enhancement of nanotubes' activity with their length can be related to several factors. First, bandgap of shorter nanotubes is wider (3.2 and 3.08 eV) compared to bandgap of nanotubes with the length of 3.5 and 6.8 μm (2.88 and 2.80 eV respectively), which suggest their lower ability to convert irradiation from visible range. Second, the surface of shorter nanotubes was covered with larger, initial amount of carbon contaminants compared with longer ones (16.0 and 12.2% vs. 6.8 and 6.7%). Comparing longer nitrogen doped nanotubes (3.5 and 6.8 μm) it was observed, that they had similar bandgap values and similar content of surface carbon contaminants. Also, the

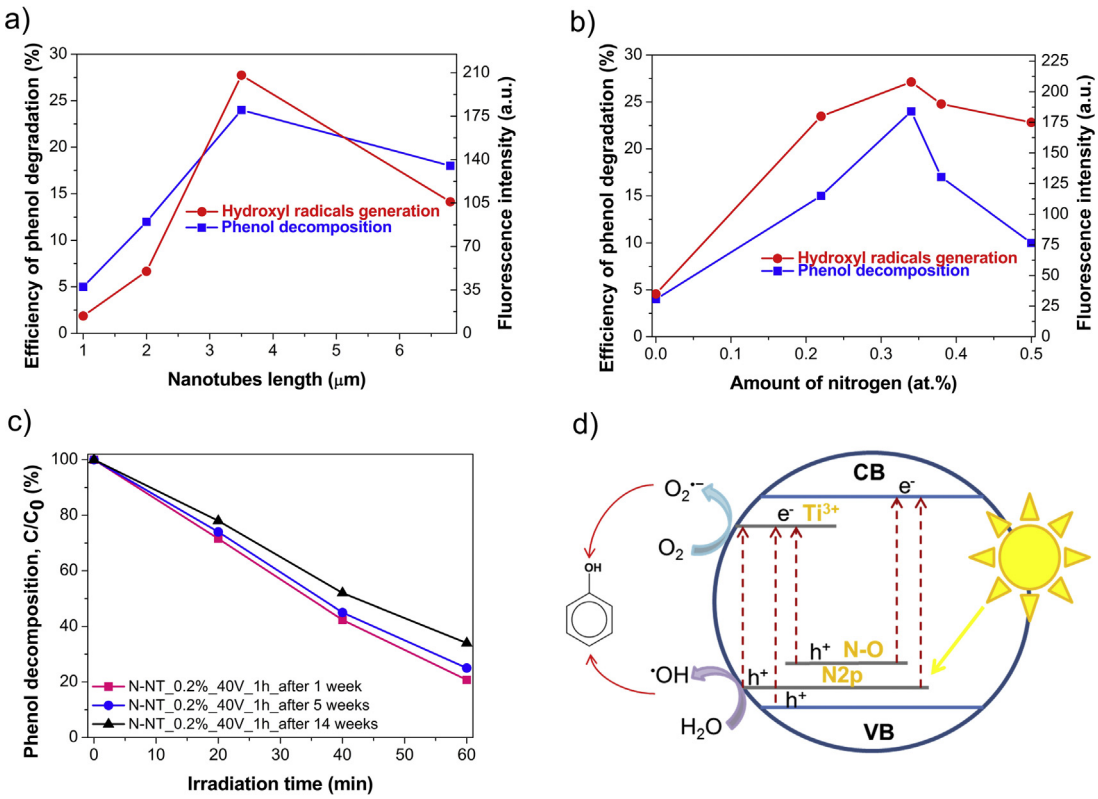

Fig. 8. Relation between photocatalytic activity of nitrogen doped TiO_2 nanotubes under visible light and nanotubes' length (a) and nitrogen dopant content (b), (c) photocatalytic decomposition of phenol under the influence of visible light irradiation on the surface of nitrogen doped TiO_2 nanotubes in the presence of scavengers (BQ—benzoquinone; TBA – *tert*-butyl alcohol), (d) mechanism of photocatalytic oxidation of phenol in presence of visible light.

content of surface —OH groups, which have a significant impact on the photocatalytic activity [68], is comparable for both samples (5.08 and 4.6% respectively). The most active sample (3.5 μm) had the larger amount of Ti^{3+} centers (3.16%) and the smallest crystallite size (27 nm). Xin et al. [69] observed, that the increase of the number of Ti^{3+} centers led to increase of photocatalytic activity of nanocrystallite TiO_2 in methylene blue decomposition in visible light. Crystallite size have also an influence on the inhibition of electron-hole recombination process and thus on the enhancement of photocatalytic activity. Jang et al. [71] observed that with the decrease of crystallite size from 30 to 15 nm, the photocatalytic activity of nanocrystallite TiO_2 in methylene blue degradation under UV irradiation increased. Zhang et al. [72] explained that in the case of well crystallized large TiO_2 particles, volume electron-hole recombination is significant type of recombination process, which can be limited by reducing of particle size. On the other hand, excessive reduction of particle size can bring out the process of surface recombination and leading to decrease of photoactivity. However, in the case of nitrogen doped nanotubes with the lengths of 3.5 and 6.8 μm the influence of the amount of Ti^{3+} centers and crystallite size on the degree of electron-hole recombination seems to be of little importance. Photoluminescence studies show that both samples exhibit very similar, relatively low electron-hole recombination rate. Thus, another, geometrical factor deciding of the highest activity of 3.5 μm nanotubes must be crucial. Zhuang et al. [74] examined the influence of TiO_2 nanotubes' length on the photocatalytic decomposition of methyl orange. Increase of nanotubes' length from 0.4 to 3.5 μm led to initial increase of photocatalytic activity under UV light which reached a maximal value in the presence of 2.5 μm-long nanotubes. In the case of visible light irradiation, the rate of methyl orange photodegradation increased with the increasing of nanotubes' length reaching approximately stable level at 2.5 μm. They explained that both, the absorption of photons and adsorption of organic pollutants increases with the increase of TiO_2 nanotubes array thickness, which is advantageous for photocatalytic process. However, when TiO_2 nanotubes film is thicker than the light penetration depth, the bottom part of film absorb small amount of incident photons and acts only as an inter-support. Moreover, the mass transfer is limited due to longer diffusion pathway which consequently lead to decrease of photocatalytic degradation rate.

The efficiency of degradation of phenol and efficiency of generation of •OH radicals under the influence of Vis irradiation in the presence of nanotubes with similar length (about 3.4 μm) but different nitrogen content (0–0.5 at.%, confirmed by XPS analysis) is presented in Fig. 8b. Photocatalytic activity significantly increased with the increase of nitrogen content, reaching maximum ($r = 1.33 \mu mol\ dm^{-3}\ min^{-1}$) for sample containing 0.34 at.% of nitrogen. According to experimental data, the undoped sample had relatively high value of bandgap (3.05 eV), relatively small amount of Ti^{3+} forms (2.88 at.%), the highest concentration of carbon contaminants (10.9 at.%) and the highest crystallites' size, which, in general, resulted in the lowest activity of this sample among all discussed ones. The most active sample had medium nitrogen content (0.34 at.%), high but not the highest amount of Ti^{3+} forms (3.16 at.%) and —OH groups (5.08 at.%). However, it possessed the smallest content of carbon contaminants (6.8%) and the smallest crystallites' size (27 nm). Similar correlation was observed by Li et al. [75]. In their case, the most active sample had relatively low nitrogen content (compared to all examined samples) but the smallest crystallites' and pores' size. Nassoko et al. [76] examined N-doped TiO_2 nanoparticles in the process of visible light photocatalytic degradation of rhodamine-B and benzene. The sample possessing medium nitrogen content exhibited the highest ability of electron-hole sep-

aration (confirmed by photoluminescence study) and was the most photocatalytically active which was associated with high visible light absorption and high surface area.

In order to determine what type of active species is responsible for decomposition of phenol under the influence of visible light irradiation over nitrogen doped TiO_2 nanotubes, the trapping experiments were performed. As the most representative sample, N—NT_0.2%_40V_1 h (the most active photocatalyst) was chosen. It has been previously proven that such scavengers like *tert*-butyl alcohol (TBA) [77] and benzoquinone (BQ) [78] have ability to trap hydroxyl radicals and superoxide radicals, respectively, and these scavengers can be applied for evaluation of the origin of the photocatalytic activity. As shown in Fig. 8c, adding each scavenger separately caused the significant decrease of phenol decomposition efficiency (decrease of 6 and 14% in the presence of superoxide and hydroxyl radicals scavengers, respectively), which suggests that not only •OH but also $O_2^{\bullet -}$ radicals are responsible for visible light photocatalytic degradation of phenol.

Based on the experimental results presented above and literature data, the probable mechanism of photocatalytic oxidation of phenol under visible light is shown in Fig. 8d. As a consequence of nitrogen doping, the bandgap is narrowed as a result of existence of substitutional (N2*p* localized states) and interstitial (N—O band) levels located above the valence band edge of TiO_2 in prepared nanotubes. Furthermore Ti^{3+} can reduce oxygen dissolved in water and produce superoxide radicals. Under visible light irradiation, photogenerated electrons can migrate from the valence band, N2*p* energy level and N—O band into the conduction band and impurity level band (associated with the presence of Ti^{3+} states), leaving positive holes in valence band, N2*p* energy level and N—O. At the same time, photogenerated electrons can reduce oxygen and produce a superoxide radical, while positive holes may be involved in generation of •OH radicals.

4. Conclusions

In summary, nanotubes having approximately the same length but various nitrogen content differ, among others, with bandgap value, crystallite size and Ti^{3+} state content which results in differences in photoactivity. Similarly, in the case of nanotubes with different length but having the same amount of nitrogen dopant, the most crucial points affecting photocatalytic activity and ability to create hydroxyl radicals are crystallite size and content of −OH groups and Ti^{3+} states. Additionally, as a consequence of nitrogen doping, visible light photoactivity is caused as a result of existence of substitutional (N2*p* localized states) and interstitial (N—O band) levels localized above the valence band of TiO_2 nanotubes. Under visible light irradiation, not only •OH but also $O_2^{\bullet -}$ radicals are responsible for photocatalytic degradation of phenol. Nitrogen doped samples showed better photocatalytic stability compared to undoped one which may be related to its better activity in first measurement cycle and consequently with better efficiency in phenol degradation byproducts removal. On the other hand, one of the most crucial factors having a negative impact on photocatalytic properties of nitrogen doped TiO_2 nanotubes is the presence of carbon species, whose amount increased with the time of exposure to ambient air, blocking photocatalyst's surface and, as a consequence, can cause decreasing its activity.

Acknowledgement

This work was supported by the Polish National Science Centre (contract No.: 2011/01/N/ST5/05540).

Appendix A. Supplementary data

Supplementary data associated with this article can be found, in the online version, at http://dx.doi.org/10.1016/j.apcatb.2016.05.006.

References

[1] K. Lee, A. Mazare, P. Schmuki, Chem. Rev. 114 (2014) 9385–9454.
[2] P. Roy, D. Kim, K. Lee, E. Spiecker, P. Schmuki, Nanoscale 2 (2010) 45–59.
[3] D. Kowalski, D. Kim, P. Schmuki, Nano Today 8 (2013) 235–264.
[4] R.P. Antony, T. Mathews, J.A. Johnson, D.N. Krishna, S. Dash, A.K. Tyagi, Energy Environ. Focus 2 (2013) 139–148.
[5] M. Nischk, P. Mazierski, M. Gazda, A. Zaleska, Appl. Catal. B: Environ. 144 (2014) 674–685.
[6] J. Podporska-Carroll, E. Panaitescu, B. Quilty, L. Wang, L. Menon, S.C. Pillai, Appl. Catal. B: Environ. 176–177 (2015) 70–75.
[7] N.T. Nguyen, J. Yoo, M. Altomare, P. Schmuki, Chem. Commun. 50 (2014) 9653–9656.
[8] R.P. Antony, T. Mathews, C. Ramesh, N. Murugesan, A. Dasgupta, S. Dhara, S. Dash, A.K. Tyagi, Int. J. Hydrogen Energy 37 (2012) 8268–8276.
[9] L.K. Preethi, R.P. Antony, T. Mathews, S.C.J. Loo, L.H. Wong, S. Dash, A.K. Tyagi, Int. J. Hydrogen Energy 41 (2016) 5865–5877.
[10] Q. Li, L. Zong, C. Li, J. Yang, Appl. Surf. Sci. 319 (2014) 16–20.
[11] X. Zhou, N.T. Nguyen, S. Özkan, P. Schmuki, Electrochem. Commun. 46 (2014) 157–162.
[12] M.M. Momeni, Y. Ghayeb, J. Electroanal. Chem. 751 (2015) 43–48.
[13] R. Yuan, B. Zhou, D. Hua, C. Shi, J. Hazard. Mater. 262 (2013) 527–538.
[14] G.G. Bessegato, J.C. Cardoso, M.V.B. Zanoni, Catal. Today 240 (Part A) (2015) 100–106.
[15] L. Sun, J. Cai, Q. Wu, P. Huang, Y. Su, C. Lin, Electrochim. Acta 108 (2013) 525–531.
[16] R.P. Antony, T. Mathews, S. Dash, A.K. Tyagi, J. Phys. Chem. C 117 (2013) 6851–6860.
[17] Q. Zheng, H. Kang, J. Yun, J. Lee, J.H. Park, S. Baik, ACS Nano 5 (2011) 5088–5093.
[18] J. Lv, H. Gao, H. Wang, X. Lu, G. Xu, D. Wang, Z. Chen, X. Zhang, Z. Zheng, Y. Wu, Appl. Surf. Sci. 351 (2015) 225–231.
[19] L. Long, J. Li, L. Wu, X. Li, Mater. Sci. Semicond. Process. 26 (2014) 107–111.
[20] H. Sun, B. Dong, G. Su, R. Gao, W. Liu, L. Song, L. Cao, Appl. Surf. Sci. 343 (2015) 181–187.
[21] R. Asahi, T. Morikawa, T. Ohwaki, K. Aoki, Y. Taga, Science 293 (2001) 269–271.
[22] R. Asahi, T. Morikawa, H. Irie, T. Ohwaki, Chem. Rev. 114 (2014) 9824–9852.
[23] L.G. Devi, R. Kavitha, Appl. Catal. B: Environ. 140–141 (2013) 559–587.
[24] A. Ghicov, J.M. Macak, H. Tsuchiya, J. Kunze, V. Haeublein, S. Kleber, P. Schmuki, Chem. Phys. Lett. 419 (2006) 426–429.
[25] X. Hou, F. Liu, K. Yao, H. Ma, J. Deng, D. Li, B. Liao, Mater. Lett. 124 (2014) 101–104.
[26] B. Yuan, Y. Wang, H. Bian, T. Shen, Y. Wu, Z. Chen, Appl. Surf. Sci. 280 (2013) 523–529.
[27] H. Chen, K.-F. Chen, S.-W. Lai, Z. Dang, Y.-P. Peng, Sep. Purif. Technol. 146 (2015) 143–153.
[28] J. Xu, Y. Ao, M. Chen, D. Fu, Appl. Surf. Sci. 256 (2010) 4397–4401.
[29] X. Hou, C.-W. Wang, W.-D. Zhu, X.-Q. Wang, Y. Li, J. Wang, J.-B. Chen, T. Gan, H.-Y. Hu, F. Zhou, Solid State Sci. 29 (2014) 27–33.
[30] Y.-K. Lai, J.-Y. Huang, H.-F. Zhang, V.-P. Subramaniam, Y.-X. Tang, D.-G. Gong, L. Sundar, L. Sun, Z. Chen, C.-J. Lin, J. Hazard. Mater. 184 (2010) 855–863.
[31] C.-W. Wang, W.-D. Zhu, J.-B. Chen, X. Hou, X.-Q. Zhang, Y. Li, J. Wang, F. Zhou, Thin Solid Films 556 (2014) 440–446.
[32] L. Dong, G.-x. Cao, Y. Ma, X.-l. Jia, G.-t. Ye, S.-k. Guan, Trans. Nonferrous Metals Soc. China 19 (2009) 1583–1587.
[33] S.-I. In, P.C.K. Vesborg, B.L. Abrams, Y. Hou, I. Chorkendorff, J. Photochem. Photobiol. A: Chem. 222 (2011) 258–262.
[34] R.P. Antony, T. Mathews, P.K. Ajikumar, D.N. Krishna, S. Dash, A.K. Tyagi, Mater. Res. Bull. 47 (2012) 4491–4497.
[35] Y. Su, X. Zhang, M. Zhou, S. Han, L. Lei, J. Photochem. Photobiol. A: Chem. 194 (2008) 152–160.
[36] D. Kim, S. Fujimoto, P. Schmuki, H. Tsuchiya, Electrochem. Commun. 10 (2008) 910–913.
[37] X. Liu, Z. Liu, J. Zheng, X. Yan, D. Li, S. Chen, W. Chu, J. Alloys Compd. 509 (2011) 9970–9976.
[38] K. Shankar, K.C. Tep, G.K. Mor, C.A. Grimes, J. Phys. D: Appl. Phys. 39 (2006) 2361.
[39] S. Liu, L. Yang, S. Xu, S. Luo, Q. Cai, Electrochem. Commun. 11 (2009) 1748–1751.
[40] A. Ghicov, J.M. Macak, H. Tsuchiya, J. Kunze, V. Haeublein, L. Frey, P. Schmuki, Nano Lett. 6 (2006) 1080–1082.
[41] B. Ohtani, J. Photochem. Photobiol. C: Photochem. Rev. 11 (2010) 157–178.
[42] J. Reszczyńska, T. Grzyb, J.W. Sobczak, W. Lisowski, M. Gazda, B. Ohtani, A. Zaleska, Appl. Catal. B: Environ. 163 (2015) 40–49.
[43] D. Regonini, A. Satka, A. Jaroenworaluck, D.W.E. Allsopp, C.R. Bowen, R. Stevens, Electrochim. Acta 74 (2012) 244–253.

[44] E. Ngaboyamahina, H. Cachet, A. Pailleret, E.M.M. Sutter, Electrochim. Acta 129 (2014) 211–221.
[45] J.M. Macak, H. Hildebrand, U. Marten-Jahns, P. Schmuki, J. Electroanal. Chem. 621 (2008) 254–266.
[46] N.-S. Peighambardoust, F. Nasirpouri, Surf. Coat. Technol. 235 (2013) 727–734.
[47] G.K. Mor, O.K. Varghese, M. Paulose, K. Shankar, C.A. Grimes, Sol. Energy Mater. Sol. Cells 90 (2006) 2011–2075.
[48] D.O. Scanlon, C.W. Dunnill, J. Buckeridge, S.A. Shevlin, A.J. Logsdail, S.M. Woodley, C.R.A. Catlow, M.J. Powell, R.G. Palgrave, I.P. Parkin, G.W. Watson, T.W. Keal, P. Sherwood, A. Walsh, A.A. Sokol, Nat. Mater. 12 (2013) 798–801.
[49] S.M.W.P. Georgios, Solid State Phenom. 162 (2010) 163–177.
[50] J. Yu, X. Zhao, Q. Zhao, Thin Solid Films 379 (2000) 7–14.
[51] C. Gang Liu, Feng Li, Da-Wei Wang, Dai-Ming Tang, Chang Liu, Xiuliang Ma, Gao Qing, Lu Hui-Ming, Nanotechnology 19 (2008) 025606.
[52] T.I.T. Okpalugo, P. Papakonstantinou, H. Murphy, J. McLaughlin, N.M.D. Brown, Carbon 43 (2005) 153–161.
[53] A.K.-V. Alexander, V. Naumkin, Stephen W. Gaarenstroom, Cedric J. Powell, NIST X-ray Photoelectron Spectrosc. Database (2012).
[54] Y. Chen, S. Zhang, Y. Yu, H. Wu, S. Wang, B. Zhu, W. Huang, S. Wu, J. Dispers. Sci. Technol. 29 (2008) 245–249.
[55] X. Chen, C. Burda, J. Phys. Chem. B 108 (2004) 15446–15449.
[56] M. Sathish, B. Viswanathan, R.P. Viswanath, C.S. Gopinath, Chem. Mater. 17 (2005) 6349–6353.
[57] Y. Cong, J. Zhang, F. Chen, M. Anpo, J. Phys. Chem. C 111 (2007) 6976–6982.
[58] M. Bellardita, M. Addamo, A. Di Paola, L. Palmisano, A.M. Venezia, Phys. Chem. Chem. Phys. 11 (2009) 4084–4093.
[59] Y.K. Lai, L. Sun, C. Chen, C.G. Nie, J. Zuo, C.J. Lin, Appl. Surf. Sci. 252 (2005) 1101–1106.
[60] G.K. Mor, O.K. Varghese, M. Paulose, C.A. Grimes, Adv. Funct. Mater 15 (2005) 1291–1296.
[61] H. Tang, H. Berger, P.E. Schmid, F. Lévy, Solid State Commun. 92 (1994) 267–271.
[62] F.J. Knorr, C.C. Mercado, J.L. McHale, J. Phys. Chem. C 112 (2008) 12786–12794.
[63] D. Regonini, C.R. Bowen, A. Jaroenworaluck, R. Stevens, Mater. Sci. Eng.: R: Rep. 74 (2013) 377–406.
[64] X. Hou, C.-W. Wang, W.-D. Zhu, X.-Q. Wang, Y. Li, J. Wang, J.-B. Chen, T. Gan, H.-Y. Hu, F. Zhou, Solid State Sci. 29 (2014) 27–33.
[65] Y. Su, Y. Xiao, X. Fu, Y. Deng, F. Zhang, Mater. Res. Bull. 44 (2009) 2169–2173.
[66] S.T. Nishanthi, S. Iyyapushpam, B. Sundarakannan, E. Subramanian, D. Pathinettam Padiyan, Appl. Surf. Sci. 313 (2014) 449–454.
[67] J.M. Macak, M. Zlamal, J. Krysa, P. Schmuki, Small 3 (2007) 300–304.
[68] J. Reszczyńska, T. Grzyb, Z. Wei, M. Klein, E. Kowalska, B. Ohtani, A. Zaleska-Medynska, Appl. Catal. B: Environ. 181 (2016) 825–837.
[69] X. Xin, T. Xu, J. Yin, L. Wang, C. Wang, Appl. Catal. B: Environ. 176–177 (2015) 354–362.
[71] H. Jang, S.-K. Kim, S.-J. Kim, J. Nanopart. Res. 3 (2001) 141–147.
[72] Z. Zhang, C.-C. Wang, R. Zakaria, J.Y. Ying, J. Phys. Chem. B 102 (1998) 10871–10878.
[74] H.-F. Zhuang, C.-J. Lin, Y.-K. Lai, L. Sun, J. Li, Environ. Sci. Technol. 41 (2007) 4735–4740.
[75] X. Li, P. Liu, Y. Mao, M. Xing, J. Zhang, Appl. Catal. B: Environ. 164 (2015) 352–359.
[76] D. Nassoko, Y.-F. Li, H. Wang, J.-L. Li, Y.-Z. Li, Y. Yu, J. Alloys Compd. 540 (2012) 228–235.
[77] N. Zhang, Y. Zhang, M.-Q. Yang, Z.-R. Tang, Y.-J. Xu, J. Catal. 299 (2013) 210–221.
[78] T.B. Li, G. Chen, C. Zhou, Z.Y. Shen, R.C. Jin, J.X. Sun, Dalton Trans. 40 (2011) 6751–6758.